

MIT Open Access Articles

ClpP1P2 peptidase activity promotes biofilm formation in Pseudomonas aeruginosa

The MIT Faculty has made this article openly available. **Please share** how this access benefits you. Your story matters.

Citation: Mawla, Gina D., Hall, Branwen M., Cárcamo#Oyarce, Gerardo, Grant, Robert A., Zhang, Jia Jia et al. 2020. "ClpP1P2 peptidase activity promotes biofilm formation in Pseudomonas aeruginosa." Molecular Microbiology, 115 (6).

As Published: <http://dx.doi.org/10.1111/mmi.14649>

Publisher: Wiley

Persistent URL: <https://hdl.handle.net/1721.1/140525>

Version: Author's final manuscript: final author's manuscript post peer review, without publisher's formatting or copy editing

Terms of use: Creative Commons Attribution-Noncommercial-Share Alike



PROF. TANIA A. BAKER (Orcid ID : 0000-0002-0737-3411)

Article type : Research Article

ClpP1P2 peptidase activity promotes biofilm formation in *P. aeruginosa*

Gina D. Mawla¹, Branwen M. Hall¹, Gerardo Cárcamo-Oyarce², Robert A. Grant¹, Jia Jia Zhang¹, Julia R. Kardon^{1‡}, Katharina Ribbeck², Robert T. Sauer¹, and Tania A. Baker^{1*}

¹Department of Biology, Massachusetts Institute of Technology, Cambridge, MA 02139

²Department of Biological Engineering, Massachusetts Institute of Technology, Cambridge, MA 02139

‡ present address: Department of Biochemistry, Brandeis University, Waltham, MA 02454

This is the author manuscript accepted for publication and has undergone full peer review but has not been through the copyediting, typesetting, pagination and proofreading process, which may lead to differences between this version and the [Version of Record](#). Please cite this article as [doi: 10.1111/MMI.14649](#)

This article is protected by copyright. All rights reserved

*Correspondence: tabaker@mit.edu

Running title: Specialized function of *P. aeruginosa* ClpP2

Keywords: ClpP protease; *P. aeruginosa*; biofilms; ClpP2; AAA+ protease; peptide cleavage specificity

Summary

Caseinolytic proteases (Clp) are central to bacterial proteolysis and control cellular physiology and stress responses. They are composed of a double-ring compartmentalized peptidase (ClpP) and a AAA+ unfoldase (ClpX or ClpA/ClpC). Unlike many bacteria, the opportunistic pathogen *P. aeruginosa* contains two ClpP homologs: ClpP1 and ClpP2. The specific functions of these homologs, however, are largely elusive. Here, we report that the active form of PaClpP2 is a part of a heteromeric PaClpP1₇P2₇ tetradecamer that is required for proper biofilm development. PaClpP1₁₄ and PaClpP1₇P2₇ complexes exhibit distinct peptide cleavage specificities and interact differentially with *P. aeruginosa* ClpX and ClpA. Crystal structures reveal that PaClpP2 has non-canonical features in its N- and C-terminal regions that explain its poor interaction with unfoldases. However, experiments *in vivo* indicate that the PaClpP2 peptidase active site uniquely contributes to biofilm development. These data strongly suggest that the specificity of different classes of ClpP peptidase subunits contributes to the biological outcome of proteolysis. This specialized role of PaClpP2 highlights it as an attractive target for developing antimicrobial agents that interfere specifically with late-stage *P. aeruginosa* development.

Introduction

Regulated protein degradation is central to bacterial physiology and development, playing critical roles in establishing and maintaining appropriate levels of intracellular proteins. AAA+ (ATPases associated with diverse cellular activities) proteases of the Clp family are macromolecular complexes conserved in bacteria and in some eukaryotic organelles. They are composed of a self-compartmentalized tetradecameric peptidase, ClpP, in complex with a hexameric AAA+ unfoldase (ClpA or ClpX in *Escherichia coli* and *Pseudomonas aeruginosa*). Clp protease substrates include proteins that regulate cellular stress responses, cell division, antibiotic resistance, motility, and virulence (Gur et al., 2011; Culp and Wright, 2017). Substrates destined for degradation are recognized and unfolded in an energy-dependent process by the unfoldase and then translocated into the central chamber of ClpP, where they are degraded into short peptides (Sauer and Baker, 2011; Baker and Sauer, 2012) (Fig. 1 A, B).

Most Proteobacteria, including *E. coli*, contain a single *clpP* gene, which is transcribed, translated, and processed to remove a propeptide. ClpP subunits assemble into inactive heptameric rings, which then associate to form a functional homomeric tetradecamer. However, organisms from phyla including Actinobacteria, Cyanobacteria, Firmicutes, and Chlamydiae frequently harbor two or more *clpP* genes, which assemble into active heteromeric tetradecamers in some cases (Akopian et al., 2012; Stanne et al., 2007; Dahmen et al., 2015; Pan et al., 2019). The specific biological advantages provided by heteromeric ClpP complexes are poorly understood. Here, we investigate the assembly, structures, activities, and biological roles of ClpP1 and ClpP2 from *P. aeruginosa*. Our results provide insight into the potential biological benefits of having two ClpP isoforms.

The substrate specificity of Clp-family proteases is determined by the AAA+ unfoldase, which recognizes specific peptide sequences (degron tags) on cognate substrates. After substrate recognition, the AAA+ enzyme uses the energy of ATP hydrolysis to unfold and then translocate the polypeptide into ClpP for degradation (Baker and Sauer, 2012). Binding of the AAA+ enzyme to ClpP involves two key interactions: (i) docking of the IGF/IGL loops of ClpX/A into specific hydrophobic pockets on the ClpP surface, and (ii) contacts between N-terminal axial loops of ClpP and pore-2 loops of the unfoldase (Kim et al., 2001; Joshi et al., 2004; Bewley et al., 2006; Gribun et al., 2005; Alexopoulos et al., 2012; Fei et al., 2020; Gatsogiannis et al., 2019; Ripstein et al., 2020; Lopez et al., 2020). Unfoldase-ClpP interaction triggers expansion of the ClpP axial pores,

allowing polypeptides to enter the proteolytic chamber. In the ClpP chamber, active sites containing a Ser-His-Asp catalytic triad cleave translocated polypeptides into ~8-10 amino acid-long peptides (Thompson et al., 1994). Thus, through coordinated action, the Clp-family protease complex chooses substrates, unfolds them, and cleaves them into short peptides (Fig. 1A, B).

The opportunistic pathogen *P. aeruginosa* is a Gram-negative bacterium that causes serious chronic infections in immunocompromised patients and is a major factor in the mortality of patients with cystic fibrosis (Lyczak et al., 2000; Gellatly and Hancock, 2013). The bacterium's ability to switch from free-swimming planktonic cells to surface-attached biofilm communities contributes to both antibiotic resistance and pathogenicity (Drenkard and Ausubel, 2002; Mah et al., 2003). *P. aeruginosa* contains two *clpP* genes located at distinct genomic loci: *clpP1* (PA1801) is in the same operon as *clpX*, as is common in many bacteria, whereas *clpP2* (PA3326) is at a locus within a cluster of genes that appear to form a mobile genetic island. The *clpP1* and *clpP2* genes also exhibit distinct expression patterns. The *clpP1* gene is expressed throughout growth whereas *clpP2* is tightly controlled by quorum sensing signaling molecules and the LasR transcription factor (Wagner et al., 2003; Schuster et al., 2003; Arevalo-Ferro et al., 2003; Hentzer et al., 2003; Gilbert et al., 2009). Genetic studies implicate both *clpP1* and *clpP2* in virulence, and deletion of either gene results in distinct cellular phenotypes (Qiu et al., 2008; Hall et al., 2017). Purified *P. aeruginosa* ClpP1 is tetradecamer that is active both as a stand-alone peptidase that cleaves very short peptides and as a protease when combined with ClpX or ClpA. ClpP2, however, purifies as a catalytically inactive heptamer, and thus its active form has remained mysterious (Hall et al., 2017).

Here, we demonstrate that a heptameric ring of PaClpP2 assembles with a heptameric ring of PaClpP1 to form an active tetradecameric complex. Using biochemical, crystallographic, and microbiological assays, we provide evidence that PaClpP1P2 hetero- and PaClpP1 homocomplexes have distinct peptidase and protease activities. Furthermore, we show that PaClpP2 peptidase activity is specifically required for normal biofilm thickness, with only thin biofilms forming in its absence. We discuss our findings in the context of models for how PaClpP1 and PaClpP2 contribute to pathogenicity and poor patient prognosis during *P. aeruginosa* infections.

Results

P. aeruginosa ClpP1 and ClpP2 form a heteromeric complex in vivo.

In a previous study characterizing the isoforms encoded by *P. aeruginosa* genes *clpP1* (PA1801) and *clpP2* (PA3326), PaClpP1 and PaClpP2 were purified after heterologous expression in *E. coli* (Hall et al., 2017). PaClpP1 purified as an active tetradecamer, whereas PaClpP2 was an inactive heptamer. We sought here to determine the active form of PaClpP2 by isolating it in native complexes from *P. aeruginosa* cells.

We specifically tested the possibility that PaClpP2 exists in a co-complex with PaClpP1, as similar heterocomplexes have been characterized from other bacterial species that carry multiple *clpP* genes (Akopian et al., 2012; Stanne et al., 2007; Dahmen et al., 2015; Pan et al., 2019). To probe for interactions between PaClpP1 and PaClpP2 in *P. aeruginosa* strain PAO1, we appended a FLAG-tag to the chromosomal copy of *clpP2*. The cellular extract was made from stationary-phase PAO1 and captured proteins were observed by stained SDS-PAGE (Fig. 1C). Two similarly sized protein bands were evident: one consistent with the size of PaClpP2-FLAG and one consistent with the size of native PaClpP1. The identity of PaClpP1 was verified by western blot following SDS-PAGE using an antibody specific for PaClpP1, as well as directly by mass spectrometry (Fig. 1D and Fig. S2). We conclude that PaClpP1 and PaClpP2 interact in *P. aeruginosa* cells.

To purify larger amounts of the PaClpP1P2 co-complex for biochemical analysis, a dual-expression plasmid encoding both ClpP forms (affinity-tagged PaClpP1-His₆ and PaClpP2-StrepII) was used for co-expression in *E. coli*. The co-complex was purified using tandem Ni²⁺-NTA and streptavidin columns in series, followed by size-exclusion chromatography (Fig. S1). The final column yielded a single peak, which eluted at the size expected for a tetradecamer (~320 kDa) and contained both PaClpP1-His₆ and PaClpP2-StrepII (Fig. 1E, F). Quantification of bands in stained gels of the purified co-complex indicated that the two ClpP isoforms were present in an approximate 1:1 ratio. Formation of PaClpP1P2 complexes strictly depended upon co-expression and co-purification; as mixing of separately purified PaClpP1 and PaClpP2 did not result in heterocomplex formation (Hall et al., 2017).

To explore the subunit arrangement within PaClpP1₇P2₇ complexes, we took two experimental approaches. First, we carried out a glutaraldehyde crosslinking time course with three separate samples: (i) PaClpP1₁₄, (ii) PaClpP2₇, and (iii) purified PaClpP1P2 co-complexes. Crosslinked samples were then analyzed by Coomassie-stained SDS-PAGE. Interestingly, the time-dependent crosslinking of PaClpP1P2 generated a gel pattern that resembled the sum of the gel patterns observed during PaClpP1₁₄ crosslinking (rapid but incomplete dimer formation) and during PaClpP2₇ crosslinking (a ladder of cross-linked species that continually formed over ~15 min) (Fig. S3). This result is consistent with the model that the PaClpP1P2 tetradecamer is composed of one homogenous PaClpP1 heptamer and one homogenous PaClpP2 heptamer, as the PaClpP1P2 crosslinking pattern highly resembled the sum of the behavior of the two subtypes.

To further probe the assembly architecture of PaClpP1P2, we took advantage of the previous observation that tetradecameric ClpP can often be disassembled into its two constitutive heptamers by incubation in certain salt solutions (Maurizi et al., 1998). Thus, after incubation of ClpP1P2 under these dissociation conditions, the resulting heptamers were isolated by size-exclusion chromatography, subjected to StrepII-affinity purification, and analyzed by SDS-PAGE (Fig. S4). This approach allows for selective capture of dissociated heptamers that contained PaClpP2-StrepII. Notably, PaClpP1-His did not bind the Strep-tactin column and was recovered in the flow-through and wash fractions (Fig. S4). In contrast, PaClpP2-StrepII initially bound to the column but was clearly observed after biotin-specific elution. The discrete recovery of PaClpP1-His in the wash fraction versus PaClpP2-StrepII in the elution fraction of this affinity column, combined with their crosslinking patterns, indicate that the two heptameric rings in PaClpP1P2 are each composed of a single detectable ClpP subtype: PaClpP1₇ or PaClpP2₇. These data, together with the ~1:1 stoichiometry of the two ClpP isoforms in the heterocomplex (Fig. 1), support a configuration of two stacked homo-heptameric rings: one of PaClpP1 and one of PaClpP2. Hereafter, this complex is referred to as PaClpP1₇P2₇. These results, together with the previous characterization of PaClpP1₁₄, allow us to conclude that *P. aeruginosa* makes two forms of ClpP tetradecamers during its life cycle: PaClpP1₁₄ and PaClpP1₇P2₇.

Crystal structures of PaClpP1 and PaClpP2 reveal key distinguishing features.

PaClpP1 and PaClpP2 share 74% and 40% sequence identity, respectively, with *E. coli* ClpP (Fig. S5). To better understand the molecular differences between the PaClpP1 and PaClpP2 peptidase subunits, we solved crystal structures of PaClpP1 and PaClpP2 to resolutions of 2.6 Å and 2.0 Å, respectively (Table S1; PDB: 5BQV and 5BQW). PaClpP1 crystallized as tetradecamer, one of its biologically relevant assemblies. PaClpP2 crystallized as a heptamer. A crystallographic 2-fold axis did generate a PaClpP2 14-mer, but we were unable to isolate a PaClpP2 tetradecamer from cells or assemble this form *in vitro*, placing into question the biological relevance of a PaClpP2 tetradecamer. Furthermore, despite significant effort, we were unable to grow high-quality crystals of the PaClpP1₇P2₇ complex. Nonetheless, analysis of our crystal structures revealed important structural differences between PaClpP1 and PaClpP2.

As expected, PaClpP1 shared high structural similarity with *E. coli* ClpP (C α RMSD = 0.43 Å) and adopted the more extended conformation of ClpP barrel structures (~100 Å high, ~100 Å wide) described previously (Kimber et al., 2010; Liu et al., 2014). PaClpP2 formed a tetradecamer by crystallographic symmetry. Although we have no evidence that this protein assembly/conformation is biologically relevant, it is nonetheless useful in visualizing the similarities and differences between PaClpP1 and PaClpP2. The tetradecamer of PaClpP2 observed in the crystal adopted a more compressed barrel conformation than the active PaClpP1₁₄ (~90 Å high, ~102 Å wide) (Fig. 2A, B). Furthermore, although the overall conformations of individual PaClpP1 and PaClpP2 subunits and rings were similar, three major differences were notable.

First, residues 4-8 and 18-20 of PaClpP1₁₄ formed a β hairpin (residues 9-17 were disordered), whereas residues 14-20 of PaClpP2₇ formed an α helix that pointed downwards into and closed the axial pore (Fig. 2B, D). N-terminal β -hairpin loops are observed in numerous ClpP structures (Kang et al., 2004; Gribun et al., 2005; Bewley et al., 2006), and their detailed conformations determine the size of the axial ClpP pore. These loops also make contacts with ClpX and ClpA in recent cryo-EM structures (Fei et al., 2020; Gatsogiannis et al., 2019; Ripstein et al., 2020; Lopez et al., 2020). A second structural difference was observed near the hydrophobic pockets where critical peptidase-unfoldase interactions occur. These pockets serve as docking sites for the

IGF/IGL loops of ClpX/ClpA, which are essential for complex formation with ClpP (Amor et al., 2019; Fei et al., 2020; Lopez et al., 2020; Gatsogiannis et al., 2019). Interestingly, the most C-terminal segment of PaClpP2 formed a single helical turn that protruded over its adjacent hydrophobic pocket (Fig. 2E) in a position that would likely interfere with ClpX/ClpA binding. Thus, structural differences near both the N- and C-termini of PaClpP2 suggest that it is unlikely to dock stably with a partner Clp unfoldase in the absence of major conformational changes.

The third notable difference between the PaClpP1 and PaClpP2 structures was an alternative positioning of the active-site residues. In the PaClpP1 structure, the Ser-His-Asp catalytic triad appeared properly spaced and positioned for peptidase activity. In contrast, those in PaClpP2 were not optimally positioned (Fig. 2F). In all subunits of PaClpP2, the active site Asp¹⁷² side chain was too far (~10 Å) from the side chains of Ser⁹⁸ and His¹²³ to form an active catalytic triad (Fig. 2F). This active-site misalignment in the crystal structure is consistent with the inactivity of the PaClpP2 heptamer in solution.

ClpX engages the PaClpP1₇P2₇ complex through interactions with PaClpP1

The crystal structures reveal that the two main regions where ClpPs commonly interact with the AAA+ unfoldases – the ClpP N-terminal loop and its hydrophobic binding pocket – are notably altered in PaClpP2. These structural features suggest that PaClpP2 does not interact canonically with unfoldases. Therefore, we investigated whether complexes containing ClpP1 and ClpP1P2 were active in degradation of protein substrates when partnered with the PaClpX or PaClpA unfoldases. We performed kinetic experiments to compare the ability of PaClpX•P1₁₄ and PaClpX•P1₇P2₇ to form proteolytic complexes and degrade a degron-tagged model substrate, GFP-ssrA. In the presence of limiting concentrations of PaClpX, the K_M (~4.1 μM) and V_{max} (~1.7 min⁻¹ ClpX₆⁻¹) values for GFP-ssrA degradation by PaClpX•P1₇P2₇ were indistinguishable from those by PaClpX•P1₁₄ (Fig. 3A). Likewise, the AAA+ unfoldase PaClpA functioned similarly in complex with either ClpP1₁₄ or ClpP1₇P2₇ to degrade the model ClpAP substrate FITC-casein (Fig. 3B). Thus, unfoldases can interact with ClpP1₁₄ and ClpP1₇P2₇ and function to degrade protein substrates.

AAA+ unfoldases can dock to either one or both sides of many homomeric ClpP barrels, producing singly-capped or doubly-capped proteolytic complexes (Grimaud et al., 1998). However, the crystal structure of PaClpP₂₇ suggests that interactions between ClpX/ClpA and PaClpP₂ in the PaClpP₁₇P₂₇ hetero-tetradecamer would be disfavored in the absence of major conformational changes. To directly visualize the stoichiometry of PaClpX binding to PaClpP₁₇P₂₇, we mixed PaClpX with PaClpP₁₄ or PaClpP₁₇P₂₇ (in the presence of ATP γ S, which stabilizes complexes) and scored the number of singly-capped and doubly-capped ClpP barrels by electron microscopy. Approximately half of the PaClpX•ClpP₁₄ particles had PaClpX bound on both sides the ClpP core (Fig. 3C). In contrast, when PaClpX and PaClpP₁₇P₂₇ were mixed, only 2% of the particles had observable PaClpX on both faces, whereas 98% of the complexes were singly-capped, and the small number of doubly-capped complexes may represent PaClpX bound to low concentration of contaminating ClpP₁₄ present in the preparation. Regardless, doubly-capped PaClpP₁₇P₂₇ peptidases either do not assemble or are a very rare species.

To further probe interactions between PaClpP₁ and PaClpP₂ and the PaClpX unfoldase, we used site-directed mutagenesis. Arg¹⁹² of EcClpP is required for stable docking with EcClpX (Fei et al., 2020). We mutated the equivalent residue in PaClpP₁, Arg¹⁹⁴, to lysine (^{RK}ClpP₁). ^{RK}ClpP₁ supported very little degradation of GFP-ssrA in the presence of PaClpX (Fig. 3D) and did not bind PaClpX in electron-microscopy experiments (Fig. S6). Thus, Arg¹⁹⁴ of PaClpP₁₄ plays an important role in assembly of the PaClpX•P₁₄ complex. Moreover, purified PaClp^{RK}P₁₇P₂₇ heterocomplexes also did not significantly degrade GFP-ssrA (Fig. 3D), supporting a model in which the PaClpP₂₇ face of PaClpP₁₇P₂₇ does not interact stably with PaClpX. We hypothesize that the ClpP₂₇ face is also defective in binding to the ClpA unfoldase, which uses a very similar docking mechanism to ClpX (Grimaud et al., 1998; Gribun et al., 2005; Bewley et al., 2006).

Rates of GFP-ssrA degradation were similar under conditions that favored formation of doubly-capped (PaClpX₆)₂•PaClpP₁₄ complexes or twice as many singly-capped PaClpX₆•PaClpP₁₄ complexes (Fig. 3E). This observation strongly suggests that both ClpX hexamers in these doubly-capped complexes are fully active during degradation. Similar results have been reported for *E. coli* ClpXP and ClpAP (Ortega et al., 2002; Maglica et al., 2009). Because only one PaClpX hexamer can bind ClpP₁₇P₂₇, a bivalent protease assembly would not be expected to form with

the PaClpP1P2 heterocomplex. Thus, this distinct unfoldase-binding property may contribute to the functional specialization of PaClpP1₁₄ and PaClpP1₇P2₇ complexes in *P. aeruginosa*.

ClpP2 active sites are essential for normal biofilm development in P. aeruginosa

As shown previously, deletion of *clpP1* in *P. aeruginosa* results in several cellular phenotypes including defects in cell attachment, motility, pyocyanin and pyoverdine production, and pathogenicity in a mouse model (Fernández et al., 2012; Shanks et al., 2006; Hall et al., 2017; Zhao et al., 2016). In contrast, deletion of *clpP2* specifically impairs the microcolony-formation stage of biofilm development in a flow-cell assay (Hall et al., 2017). The importance of PaClpP2 in biofilm assembly/maturation was also observed under static (non-flow) growth conditions. In this assay, biofilms formed by $\Delta clpP2$ cells were thinner than those formed by wild-type PAO1 as measured by confocal microscopy using GFP-labeled strains (Fig. 4). Thus, the *clpP2* deletion changes the three-dimensional architecture of *P. aeruginosa* biofilms, perhaps through alteration of the biofilm extracellular matrix, as regulation of alginate biosynthesis is under the control of ClpP-dependent proteolysis in some strains (Qiu et al., 2008). In contrast to the inhibitory effect of the *clpP2* mutation, deletion of *clpP1* slightly increased biofilm thickness, as reported previously (Fig. 4B; Shanks et al., 2006).

We next tested whether the peptide cleavage activity of PaClpP2 (presumably within a PaClpP1₇P2₇ heterocomplex) was important for the observed role of PaClpP2 in biofilm growth/morphology. Rather than using a strain with a *clpP2* deletion, a *clpP2*^{S98A}-*flag* allele, which encodes protein lacking the catalytic serine, was integrated at the *clpP2* locus and the biofilm growth assay was repeated (Fig. 4). This *clpP2*^{S98A} strain exhibited a similar but more severe biofilm-growth defect compared to the $\Delta clpP2$ strain, whereas the *clpP2*-*flag* control strain developed biofilms of normal thickness (Fig. 4B). This result indicates that the biofilm defect resulted from mutation of the catalytic serine residue in *clpP2*. We also confirmed through co-immunoprecipitation that PaClpP1 interacted well with PaClpP2^{S98A}-FLAG *in vivo*, strongly suggesting that expression, stability, and assembly into a heterocomplex occurred normally (Fig. 1C). These results lead us to propose that cleavage of a peptide or protein by the PaClpP2 active site influences biofilm thickness.

PaClpP2 has a distinct cleavage specificity that contributes to ClpP1₇P2₇ activity

To characterize the peptidase activity of PaClpP1₇P2₇ and compare it to that of PaClpP1₁₄, the purified enzymes were first assayed for activity against a panel of 18 short peptides each linked to a C-terminal fluorogenic AMC (7-amino-4-methylcoumarin) leaving group. Cleavage between the C-terminal amino acid and AMC results in a quantifiable fluorescent signal (Fig. 5A, left). ClpP tetradecamers without an associated AAA⁺ unfoldase can hydrolyze only short peptides that diffuse into the ClpP degradation chamber through the constricted axial pores (Maurizi et al., 1994). Both PaClpP1₁₄ and PaClpP1₇P2₇ heterocomplexes had substantial and generally similar cleavage activity against seven of the eighteen substrate peptides tested and exhibited weak cleavage activity against the remaining peptides (Fig. 5B).

However, the activities against some peptides indicated that the two complexes had different substrate preferences. Among the eight peptides robustly cleaved by the ClpP complexes, most were cleaved at a faster rate by PaClpP1₁₄ than PaClpP1₇P2₇, but two of them, GGL-AMC and LLL-AMC, were cleaved more rapidly by the heterocomplex (Fig. 5B, C). One of the weakly-cleaved substrates, LEHD-AMC, was also preferentially cleaved by PaClpP1₇P2₇. To confirm that faster GGL-AMC and LLL-AMC cleavage was mediated by PaClpP2₇ active sites, we purified and assayed PaClp^{SAP}1₇P2₇, a variant with the active-site serine residues in PaClpP1₇ replaced by alanine. PaClp^{SAP}1₇P2₇ degraded GGL-AMC and LLL-AMC well, confirming the PaClpP2₇ active sites within the heterocomplex contribute substantially to the higher cleavage rates of these substrates (Fig. 5C, D). Conversely, PaClp^{SAP}1₇P2₇ displayed poor activity against IETD, AAN, and LLE and was nearly inactive against the AAA, DEVD, and IIW substrates. We note, however, that the basal activities of both wild-type complexes were also low against IETD, LLE, and DEVD (Fig. 5B). These experiments demonstrate that the active sites of both PaClpP1 and PaClpP2 contribute to the peptide-cleavage activity of PaClpP1₇P2₇ and that the PaClpP1 and PaClpP2 rings exhibit differences in their preferred cleavage sites.

PaClpP1₁₄ and PaClpP1₇P2₇ display distinct protease cleavage patterns

We next sought to compare the cleavage specificities of the PaClpP isoforms during protein degradation (Fig. 5A, right) by analyzing the activity of the following proteolytic complexes: PaClpX•P1₁₄, PaClpX•P1₇P2₇, PaClpX•Clp^{SAP}1₇P2₇ and PaClpX•ClpP1₇^{SAP}P2₇. We used LC-

MS/MS to identify more than 13,000 cleaved peptides from four different protein substrates for each protease complex, allowing us to determine product peptide lengths and cleavage sequences. Although all four complexes generated peptides that averaged 8-11 residues in length (Fig. S7), the complexes that each contained only one active ClpP ring (PaClpX•Clp^{SAP}P1₇P2₇ and PaClpX•ClpP1₇^{SAP}P2₇) generated a statistically significantly larger pool of longer peptides (from 12-28 residues) (P value > 0.05; Fig. S7B). This observation is consistent with a previous report that inactivating the catalytic triads of EcClpP₁₄ through chemical modification leads to a shift in the product-size distribution towards longer peptides (Thompson et al., 1994).

In Figures 5E-H, the preferred sequences surrounding the cleavage sites produced by each enzyme variant are displayed as WebLogos (Crooks et al., 2004). Substrate residues surrounding the cleavage site are labeled as positions P3-P2-P1-P1'-P2'-P3', where the scissile bond is between P1-P1' (Schechter and Berger, 1967). For all four enzyme variants, the residue at P1 was most conserved (~0.54 to ~0.61 bits). However, the identity of the most preferred amino acid(s) at this position differed. For the enzyme variants that had only PaClpP1 active sites, Ala, Gly, and Leu appear equally favored (Fig. 5E, F). In contrast, cleavage by the PaClpP2 active site revealed a substantially stronger preference for Leu at the P1 site, with Phe being a less-preferred second choice (Fig. 5G). Both Ala and Gly, preferred residues at P1 for the PaClpP1 active site, were also notably less represented in sequences cleaved by PaClpP2 (Fig. 5G). The specificity for Leu at the P1 position for PaClpP2 during protein degradation is consistent with our findings from peptide degradation experiments, as GGL and LLL, which also contain Leu at the P1 position, was also preferentially cleaved by enzymes carrying active PaClp2 subunits.

Additionally, the cleavage specificity of the PaClpP2 active site appears to be more stringent than that of PaClpP1, as the residue at the P1 position dominated cleavage-site selection to a greater extent for PaClpP2 than it did for PaClpP1. This is shown by the WebLogo for PaClpX•Clp^{SAP}P1₇P2₇ (Fig. 5G), with the P1 position contributing ~0.64 bits of sequence information compared to only ~0.23 bits for each of the other positions (P3, P2, etc.). In contrast, for PaClpX•ClpP1₁₄ and PaClpX•ClpP1₇^{SAP}P2₇, which have only PaClpP1 active sites, other positions contributed as much as 0.32 bits (Fig. 5E and 5F). Importantly, the cleavage signature of PaClpP2 is evident in the WebLogo of PaClpX•ClpP1₇P2₇, as Leu is larger and above Gly and

Ala, which are preferred residues for PaClpP1. Thus, recognition/cleavage by PaClpP1₇P2₇ appears to reflect the preferences of both rings of the heterocomplex, thereby revealing that ClpP2 changes the overall specificity of the PaClpP1P2 heterocomplex. In depth analysis of the four WebLogos revealed additional differences between PaClpP1₁₄ and PaClpP1₇P2₇ at positions P2 and P1', which are highlighted in Fig. S8.

Our experiments probing peptide-cleavage specificity and biofilm formation lead to two related observations. First, PaClpP1₁₄ and PaClpP1₇P2₇ have distinct (although partially overlapping) cleavage preferences. Second, there is a unique requirement for functional ClpP2 active site for proper biofilm development. These results support a model in which preferential cleavage of a peptide or protein by ClpP2 within the heterocomplex promotes properly structured and clinically deleterious biofilm development during late stages of *P. aeruginosa* growth.

Discussion

***P. aeruginosa* makes two distinct functional ClpP peptidases during development.**

The opportunistic pathogen *P. aeruginosa* encodes and expresses two distinct homologs of ClpP peptidase subunits (Hall et al., 2017). We previously determined that PaClpP1 is expressed throughout different growth phases, assembles into functional tetradecamers, is an active peptidase, and forms a critical part of functional proteases when partnered with the PaClpX or PaClpA AAA+ unfoldase (Hall et al., 2017). In this study, we identify PaClpP2 as an active component of a functionally specialized proteolytic complex. By purifying and characterizing PaClpP2-containing complexes from native *P. aeruginosa* cultures and from *E. coli* expression strains that co-overproduce *clpP1* and *clpP2*, we identified the active form of PaClpP2 as part of a PaClpP1₇ClpP2₇ enzyme and found that this atypical ClpP homolog has distinct activities from those of ClpP1. Based on these observations, as well as expression studies showing that *clpP2* (but not *clpP1*) is induced approximately 10-fold during stationary phase when biofilms develop (Waite et al., 2006), we conclude that *P. aeruginosa* makes two distinct forms of the ClpP peptidase, PaClpP1₁₄ and PaClpP1₇ClpP2₇, during its life cycle, and these different peptidases play substantial roles in determining developmental outcomes during bacterial growth.

***PaClpP2* has distinct structural features and is related to *L. monocytogenes* ClpP1.**

PaClpP1 is a canonical member of the ClpP-peptidase family with high sequence identity and very similar biochemical properties to *E. coli* ClpP (Hall et al., 2017). PaClpP2 is more divergent in sequence and is on a distinct branch in phylogenetic trees, where it clusters with ClpP2s from close relatives of *P. aeruginosa* and with ClpP1 from the firmicute *Listeria monocytogenes* (Fig. S9). This observation suggests that PaClpP2 and LmClpP1 were likely acquired via horizontal gene transfer from a common ancestor. Indeed, PaClpP2 shares 50% identity with LmClpP1, 42% identity with *E. coli* ClpP, and only 40% identity with PaClpP1 (Fig. S5). *L. monocytogenes*, like *P. aeruginosa*, makes two types of functional ClpP enzymes: a canonical ClpP tetradecamer (LmClpP2₁₄) and a LmClpP1₇P2₇ heterocomplex (Dahmen et al., 2015).

Our structural and biochemical experiments demonstrate that the active form of PaClpP2 is a heptamer that stacks with a heptamer of PaClpP1 to form the PaClpP1₇P2₇ tetradecamer. An interesting feature of the ClpP2₇ side of this complex is that it does not interact stably with AAA+ unfoldases such as PaClpX or PaClpA. The basis for this lack of interaction is suggested by our crystal structure of PaClpP2₇, in which both the N- and C-terminal regions of each subunit adopt conformations that are predicted to be incompatible with ClpX or ClpA binding. Like PaClpP1₇P2₇, LmClpP1₇P2₇ binds asymmetrically to ClpX, with LmClpX binding to the LmClpP2₇ side (Dahmen et al., 2015), suggesting that failure to bind AAA+ unfoldases may be a property of this alternative ClpP subclass.

Models for the roles of two ClpP forms: cleavage specificity as a regulatory function?

Our new insights into *P. aeruginosa* ClpP2, together with previous studies, illuminate possible models for the biological roles of the two distinct ClpP peptidases during bacterial growth and development (Fig. 6). ClpP1₁₄ is a canonical family member: the *clpP1* gene is in an operon with *clpX* and is constitutively expressed throughout exponential and stationary phase growth. As an enzyme, PaClpP1₁₄ is an active peptidase with broad cleavage specificity and interacts with both PaClpX and PaClpA to form active proteases. These proteases can be singly- or doubly-capped by an unfoldase, and ClpP1₁₄ is twice as active when doubly-capped. PaClpP1₁₄ is thus a typical component of ClpXP and ClpAP enzymes that function in growing bacteria to identify and degrade protein-quality-control substrates, such as ssrA-tagged failed translation products, transcription factors, and other regulatory/metabolic proteins. For example, PaClpA, PaClpP1, and the ClpA-

adaptor protein (ClpS) are reported to control levels of the transcription factor CdpR, which helps to regulate production of pyocyanin, biofilm development, and pathogenicity in a mouse model for infection (Zhao et al., 2016). Interestingly, *clpP1*-defective strains show increased pyocyanin production and altered biofilm structure (thicker and fluffier), suggesting that loss of ClpP1 activity causes changes in early regulatory pathways that contribute to pathogenesis (Hall et al., 2017; this study).

The *clpP2* gene and the PaClpP1₇P2₇ enzyme exhibit several distinctive features compared to PaClpP1. Expression of *clpP2* is activated by LasR, a quorum-sensing transcription factor (Gilbert et al., 2009). As a consequence, PaClpP2 is undetectable during exponential growth but becomes abundant in stationary phase and biofilms. Furthermore, instead of clustering on the genome with other protein quality control enzymes like *clpP1*, *clpP2* maps to a gene cluster called *aze* that appears to be a mobile genetic island. Genes at this locus are also controlled by quorum sensing and have recently been shown to synthesize a modified nonribosomal peptide called azetidomonamide B or azabicyclene (Hong et al., 2019; Patteson et al., 2019). Genes homologous to *clpP2* and *aze* are clustered in several bacterial genomes, which suggests a potential functional relationship that remains to be explored.

At the level of enzyme function, two differences between PaClpP1₇P2₇ and PaClpP1₁₄ stand out. First, PaClpP2 cannot form an active protease on its own and has evolved structural features that prevent efficient AAA⁺ unfoldase interaction. Thus, to function as a protease, PaClpP2 must co-assemble with PaClpP1 to form a PaClpP1₇P2₇ heterocomplex. Degradation studies reveal that only the ClpP1 ring of this complex can bind ClpX, but that both the PaClpP1 and PaClpP2 peptidase active sites participate in protein degradation. Second, PaClpP1 and PaClpP2 have distinct amino-acid signatures in their preferred polypeptide cleavage sites. For example, we found that PaClpP1₇P2₇ preferentially cleaved substrates with Leu at the P1 position, whereas ClpP1₁₄ favored Ala and Gly (Fig. 5). The differential cleavage specificities of PaClpP1 and PaClpP2 at the P1 position likely reflect the structural properties of the PaClpP1 and PaClpP2 S1 binding pockets (Hedstrom, 2002; Szyk and Maurizi, 2006). Indeed, the S1 binding pocket of PaClpP2 contains a Phe residue (position 154) that could aid in better hydrophobic packing of substrate side-chains during peptide positioning and catalysis (Fig. S10).

These results indicate that PaClpP2 in complex with PaClpP1 imparts an altered substrate-processing activity, both to the PaClpP1₇P2₇ tetradecameric peptidase and to the associated AAA+ protease complex. Our *in vitro* results demonstrate that ClpP2 modulates both ATP-dependent and ATP-independent processing of substrates by PaClpP1₁₄, whereas the experiments *in vivo* demonstrate that growth of a normally-structured thick biofilm is dependent on PaClpP2 enzymatic activity. Taken together, these results support models that involve PaClpP1₇P2₇ specifically producing a cleavage product that has a downstream function in enhancing biofilm formation (Fig. 6B).

Multiple peptidase isoforms

While genomes encoding multiple alternative peptidase subunits for AAA+ proteases are continuing to be discovered, the immunoproteasome of jawed vertebrates is one of the best-characterized proteases containing alternative peptide isoforms and reveals a biologically important and developmentally regulated example of cells inducing expression of alternative peptidase subunits to help deal with cellular stress. In this case, in response to a challenge such as viral infection, cells induce expression of three alternative β subunits for the 20S peptidase particle. The difference in cleavage preference, especially of the alternative β 1 subunit, results in the generation of a pool of peptides that is biased away from cleavage after acidic residues and enhanced in production of peptides with N-terminal hydrophobic residues. This latter family of peptides is better suited to be displayed by the peptide-binding receptors of the immune system. This example, together with our observations indicating a distinct cleavage specificity for PaClpP2, emphasizes that the peptidase subunits of AAA+ proteases, not just the ATPase regulatory particles, can play a key and perhaps widespread role in determining the biological outcomes of protein/peptide degradation.

Acknowledgements

We thank Sora Kim and Kristin Zuromski (MIT) for providing purified protein substrates for ClpXP proteolysis and members of the Baker and Sauer labs for helpful discussions. This work was supported by NIH grants GM-101988 (RTS), AI-016892 (RTS, TAB), R01-EB017755 and ICB UARC (KR) and the Howard Hughes Medical Institute (TAB). Studies using the NE-CAT

beamline were supported by the NIGMS (P30 GM124165). The Eiger 16M detector on 24-ID-E beam line was funded by a NIH-ORIP HEI grant (S10OD021527). Use of the Advanced Photon Source at Argonne National Library was supported by the US DOE (contract DE-AC02-06CH11357).

Author Contributions

Individual authors have contributed as follows: (i) GDM, BMH, RTS, & TAB, the conception or design of the study, (ii) GDM, BMH, GC-O, RAG, JJZ, JRK, KR, RTS, & TAB, the acquisition, analysis, or interpretation of the data; and (iii) GDM & TAB, major contribution to writing of the manuscript; (iv) GDM, RTS, JRK, JJZ, & TAB, critical revisions to the manuscript.

Experimental Procedures

Strains and plasmids

PCR was carried out on *Pseudomonas aeruginosa* PAO1 genomic DNA provided by the American Type Culture Collection (ATCC). Plasmids were selected using 100 $\mu\text{g mL}^{-1}$ ampicillin, 50 $\mu\text{g mL}^{-1}$ kanamycin, 10 $\mu\text{g mL}^{-1}$ gentamicin (*E. coli*) or 30 $\mu\text{g/mL}$ gentamicin (*P. aeruginosa*) as appropriate. Deletion or allelic-exchange strains of *Pseudomonas aeruginosa* PAO1 were made with homologous recombination as described using vector pMQ30, yeast strain *S. cerevisiae* InvSc1 and *E. coli* mating strain ST18 (Hmelo et al., 2016). Briefly, pMQ30 deletion constructs were obtained by co-transforming cut pMQ30 plasmid and PCR-amplified regions flanking *P. aeruginosa* genes of interest into *S. cerevisiae* strain InvSc1. Reconstituted deletion plasmids were isolated, purified at greater concentration and transformed into *E. coli* strain ST18 for mating with *P. aeruginosa* PAO1. Genetic knock outs and allelic-exchange strains were confirmed with colony PCR. PaClpP1-His₆ and PaClpP2-StrepII were expressed in pET23b (Novagen). PaClpP1-His₆ and PaClpP2-StrepII were overexpressed from pETDuet1 vector (Novagen). PaClpX was expressed with an N-terminal thrombin-cleavable poly-histidine tag. Tagmaster Site-Directed Mutagenesis (GM Biosciences) was used to introduce point mutations. Generation of *clpP2-FLAG* (WT and S98A) variant alleles were constructed by homologous recombination as described above using the following primer sequences (5'-3'): CGCTATTACGCCAGCTGGCGAAAGGGGGA-TGTGCTGCAAGCTGCATGGCTATGCTTCAC (GM13_For) and TCGGTGTGATGAA-

GCGGATC (GM14_Rev) for amplifying the 5' upstream region of *clpP2* with 40 base pair homology to pMQ30, TATGAAAACCGATGACAAGGACC (GM15_For) and TTA CTTGT-CGTCGTCGTCCTTATAG (GM16_Rev) for amplifying *clpP2*-FLAG from a separate plasmid, GCTACCTGGTCAGGACTATAAGGACGACGACGACAAGTAAGCCGGATAAATACGAA GGC (GM17_For) and GAGCTCGGTACCCGGGGATCCTCTAGAGTCGACCTGCAGCCA- GGGATTCTCTACGAACC (GM19_Rev) for amplifying the 3' downstream region of *clpP2*, with homology to FLAG and pMQ30.

Protein expression and purification

For protein induction, PaClpP1, PaClpP2 and PaClpP1ClpP2 variants were expressed in *E. coli* strain JK10 (*clpP*⁻) grown at 37°C in Luria-Bertani (LB) broth supplemented with antibiotics. At OD₆₀₀ of 0.6, temperature was reduced to either 30°C (for PaClpP1-His₆ and PaClpP2-StrepII) or 20°C (for coexpression of PaClpP1-His₆ and PaClpP2-StrepII), isopropyl β -D-1-thiogalactopyranoside (IPTG) was added to a final concentration of 1 mM in 1 L cultures and cells were harvested after 3 h (PaClpP1-His₆ and PaClpP2-StrepII) or overnight (coexpression of PaClpP1-His₆ and PaClpP2-StrepII). For purification of PaClpP1-His₆/P2₇-StrepII, cell pellets were resuspended in Buffer S (50 mM sodium phosphate pH 8.0, 100 mM NaCl, 10% glycerol, 5 mM imidazole), lysed with French press, and cell lysate was mixed with 1% w/v CHAPS detergent for 30 min at 4°C. Lysate was then centrifuged for 20 min at 30,000 RCF, and the supernatant was applied to Ni-NTA resin equilibrated in Buffer S, washed extensively with Buffer S plus 20 mM imidazole, and protein was eluted with Buffer S plus 300 mM imidazole. The eluate was diluted 1:3 into Buffer W (100 mM Tris (pH 8.0), 150 mM NaCl, 10% glycerol) and applied to Strep-Tactin resin (IBA) equilibrated in Buffer W, and washed extensively with Buffer W. Protein was eluted with 2.5 mM Desthiobiotin (IBA) in Buffer W and concentrated by ultracentrifugation with a 30 kDa centrifugal filter (Amicon) to ~500 μ L. This material was further purified using a Superdex200 16/600 HR gel-filtration column (GE Healthcare) equilibrated in Buffer X (25 mM Tris (pH 7.5), 100 mM NaCl, 0.1 mM EDTA, 0.1 mM DTT, 10% glycerol). Fractions containing protein at >95% purity as judged by SDS-PAGE were combined, concentrated, flash frozen in aliquots, and stored at -80°C. For purification of PaClpP1-His₆ or PaClpP2₇-StrepII variants, the same experimental procedure as above was followed, except only Ni-NTA resin was used for PaClpP1-His₆ and only Strep-Tactin resin was used for PaClpP2-StrepII, followed by size-

exclusion chromatography (see above). *P. aeruginosa* ClpA was overexpressed and purified with Ni-NTA, as described for PaClpP1-His. Protein was then incubated for 2 h at 30°C with His-tagged Ulp1 to cleave between the SUMO domain and ClpA, eluted from Ni-NTA resin, dialyzed into buffer Q50 (50 mM Tris (pH 8.0), 1 mM DTT, 10 mM MgCl₂, 10% glycerol, 50 mM KCl), and purified on a Mono Q column (GE Healthcare). Selected fractions were further purified by size exclusion chromatography in Buffer Q200 (50 mM Tris (pH 8.0), 1mM DTT, 10 mM MgCl₂, 10% glycerol, 200 mM KCl). GFP with a C-terminal ssrA tag (*E. coli*) was expressed and purified as described (Dogan et al., 2002). *Note*: The C-terminal ssrA tag on GFP is the *E. coli* sequence (-AANDENYALAA). The *P. aeruginosa* ssrA sequence is very similar (-AANDDNYALAA).

Enzymatic assays and crosslinking

Protein and peptide degradation assays were carried out in 25 mM HEPES-KOH (pH 7.6), 5 mM KCl, 5 mM MgCl₂, 0.032% NP-40, and 10% glycerol (PD buffer) at 30°C. Peptidase assays used 2.85% dimethyl sulfoxide (DMSO), 100 μM fluorogenic peptide (Bachem, Peptides International, or Enzo Life Sciences), and 0.4 μM ClpP tetradecamer (PaClpP₁₄), and cleavage was monitored by fluorescence with excitation/emission 380/460 nm at 30°C. Degradation of GFP-ssrA for Michaelis-Menten analysis was monitored as described using 0.54 μM PaClpP₁₄, 0.1 μM ClpX₆, and an NADH-coupled ATP regeneration system (Nørby 1988; Oliveras et al., 2014). Enzymatic assays were monitored on a SpectraMax M5 microplate reader (Molecular Devices) in a black 384-well flat-bottom plate (Corning). For crosslinking of PaClpP complexes, 0.4 μM PaClpP₁₄ was mixed with 0.125% glutaraldehyde at room temperature, and reactions were stopped by flash-freezing after indicated time points and analyzed by SDS-PAGE. Casein fluorescein isothiocyanate (FITC-casein) was purchased from Sigma-Aldrich.

Western blotting and co-immunoprecipitation

PAO1 or *clpP2-FLAG* cultures for co-immunoprecipitation were grown overnight at 37°C shaking in LB. The next day, cells from 1 mL of culture were harvested by centrifugation (10 mins at 2,350xg), and cell pellets were lysed using B-PER bacterial protein extraction reagent (ThermoFisher). For co-immunoprecipitation of ClpP2-FLAG from *P. aeruginosa* strains, anti-FLAG M2 magnetic beads (Sigma-Aldrich) were incubated with cell lysate containing either

clpP2-1xFLAG (+) or untagged *clpP2* (-) alleles at the genomic loci, and eluted with excess 3xFLAG peptide (Sigma-Aldrich). The eluate was separated by SDS-PAGE and proteins were stained with SYPRO orange (Sigma-Aldrich). The eluate was analyzed by Western blot for PaClpP1 (1:15,000 anti-PaClp1) and PaClpP2 (1:7,500 anti-PaClpP2) as described (Hall et al., 2017). Secondary antibody was anti-rabbit IgG-alkaline phosphatase (AP) conjugate (Bio-Rad) used at a 1:10,000 dilution. Blots were incubated with AP ECF substrate (GE Healthcare) and imaged with a Typhoon FLA 9500 scanner (GE Healthcare).

Crystallography and negative-stain electron microscopy

For crystallization of PaClpP1, hanging drops with 0.5 μ L of PaClpP1P2 protein at 6.6 mg/ml in storage buffer (0.05 M Tris HCl (pH 7.5), 0.05 M NaCl, 5 mM EDTA, 25 mM DTT, 5% glycerol) were mixed with 0.5 μ L well solution (0.1 M sodium malonate, 53.5% MPD) over a reservoir of 500 mL well solution at 20°C. For crystallization of PaClpP2, hanging drops with 1.5 μ L of 32.6 mg/ml PaClpP2-StrepII in storage buffer (100 mM Tris (pH 8.0), 150 mM NaCl, 10% glycerol) and 1.5 μ L of precipitant (1.8 M sodium phosphate monobasic monohydrate, potassium phosphate dibasic, pH 6.9) were incubated over a reservoir of 500 ml precipitant at 20°C. Crystals were soaked in precipitant plus 10% ethylene glycol and frozen in liquid N₂. X-ray diffraction data were collected at the Advanced Photon Source (APS) beamline 24-ID-E with X-ray wavelength 0.9792 Å. For the PaClpP2 crystal, diffraction images were indexed, integrated and scaled using HKL2000 (Otwinoski and Minor, 1997). The structure was solved by molecular replacement with Phaser using a portion of a *S. aureus* ClpP monomer (PDB 3QWD) as the search model (McCoy et al., 2007). The asymmetric unit in the MR solution consisted of seven monomers in a heptameric ring. The PaClpP2 amino-acid sequence was inserted with Autobuild in Phenix (Adams et al., 2010), and the resulting model was refined using Coot (Emsley et al., 2010) and Phenix. For the PaClpP1 structure, diffraction data were processed using XDS (Kabsch et al., 2010) and solved by molecular replacement, using a heptameric ring derived from the *E. coli* ClpP structure (PDB 1YG6) as a search model. The model was refined by iterative rebuilding in Coot and refinement using Phenix. Coordinates for both structures were deposited in the Protein Data Bank (5BQV and 5BQW). For electron microscopy, 0.5 μ M PaClpX₆ and 0.2 μ M PaClpP₁₄ were diluted in 25 mM Hepes (pH 7.6), 100 mM KCl, 10 mM MgCl₂, 0.5 mM TCEP, 2 mM ATP γ S to achieve 18 ng/ μ L total protein. 5 μ L of this mixture was spotted per copper grid (Electron

Microscopy Sciences) and stain with 2% uranyl acetate. Images were obtained using a FEI Technai Spirit Transmission Electron microscope.

Mass spectrometry and data analysis

Protein digestion samples were resuspended to 1 mM in 2% formic acid. 1 μ L was analyzed for each sample. The sample was loaded with an autosampler directly onto the column, which was made from a 50 μ m ID 360 μ m OD capillary (PicoFrit, New Objectives, Woburn, MA) filled with 25 cm of 1.9 μ m Reprosil-Pur C18 AQ. Peptides were eluted at 200 nL min⁻¹ from the column using an EasyNanoLC (Thermo Scientific, San Jose, CA) with a gradient of 5% buffer B (80% acetonitrile, 0.1% formic acid) over 3 min, followed by 5% buffer B to 25% buffer B over 20 min. The gradient was then switched from 25% to 100% buffer B over 5 min and held constant for 3 min. Finally, the gradient was changed from 100% buffer B to 100% buffer A (100% water, 0.1% formic acid) over 0.5 min and then held constant for 13.5 min. The application of a 2.0 kV distal voltage electrosprayed the eluting peptides directly into the Thermo Orbitrap QE HFX mass spectrometer equipped with a Flex Source (Thermo Scientific). Mass spectrometer-scanning functions and HPLC gradients were controlled by the Xcalibur data system (Thermo Scientific). The mass spectrometer was set to scan MS1 at 60,000 resolution with an AGC target set at 3e6. The scan range was m/z¹ 375-1500. For MS2, spectra were acquired with an AGC target of 1e6 and a maximum IT at 200ms at 30,000 resolution. The top 5 peaks were analyzed by MS2. Peptides were isolated with an isolation window of m/z¹ 1.2 and fragmented at 28 CE. Only ions with a charge state of 2 and 3 were considered for MS2. Dynamic exclusion was set at 10 sec. Mass spectrometry data was analyzed with ProteomeDiscoverer 2.3 and searched against a database comprising of the four protein sequences (FNR_ECOLI, GFP_ssrA, RARC_BPP22, HTitin_HUMAN) added to an *E. coli* database (released May 14, 2019) containing common contaminant proteins. No enzyme was specified, and oxidized methionine and N-terminal acetylation were allowed as protein modifications. Only high confidence peptides from the PSM table were analyzed further. Peptides not from the four proteins analyzed were eliminated.

Biofilm assays

P. aeruginosa strains were fluorescently tagged at an intergenic neutral chromosomal locus downstream of the *glmS* gene with *egfp* in mini-Tn7 constructs as described (Lambertsen et al.,

2004; Choi et al., 2006). Overnight culture of GFP-labeled strains were prepared in LB broth with shaking at 37°C. Overnight cultures were diluted in ABTGC medium (Chua et al., 2015) to an initial OD₆₀₀ of 0.01, added to a glass-bottom 96-well plate, and incubated for 48 h at 37°C. Image acquisition was performed using a confocal laser scanning microscope (LSM 800; Zeiss) equipped with a 63×/1.4 NA oil immersion or a 100×/1.4 NA oil immersion objective. Images were analyzed with Zeiss ZEN 2.1 imaging software (Thornwood, NY, USA). The excitation wavelength for GFP was 488 nm. At least five stacks were recorded for each well and at least three independent wells were analyzed for each condition. Images were acquired with a step size of 0.5 µm. Biofilm quantification was performed using COMSTAT (Heydorn et al., 2000).

References

- Adams, P. D. *et al.* (2010) 'PHENIX: A comprehensive Python-based system for macromolecular structure solution', *Acta Crystallographica Section D: Biological Crystallography*, 66(2), pp. 213–221. doi: 10.1107/S0907444909052925.
- Akopian, T. *et al.* (2012) 'The active ClpP protease from *M. tuberculosis* is a complex composed of a heptameric ClpP1 and a ClpP2 ring', *EMBO Journal*. Nature Publishing Group, 31(6), pp. 1529–1541. doi: 10.1038/emboj.2012.5.
- Alexopoulos, J. A., Guarné, A. and Ortega, J. (2012) 'ClpP: A structurally dynamic protease regulated by AAA+ proteins', *Journal of Structural Biology*. Elsevier Inc., 179(2), pp. 202–210. doi: 10.1016/j.jsb.2012.05.003.
- Amor, A. J. *et al.* (2019) 'Roles of the ClpX IGF loops in ClpP association, dissociation, and protein degradation', *Protein Science*, 28(4), pp. 756–765. doi: 10.1002/pro.3590.
- Arevalo-Ferro, C. *et al.* (2003) 'Identification of quorum-sensing regulated proteins in the opportunistic pathogen *Pseudomonas aeruginosa* by proteomics', *Environmental Microbiology*, 5(12), pp. 1350–1369. doi: 10.1046/j.1462-2920.2003.00532.x.
- Baker, T. A. and Sauer, R. T. (2012) 'ClpXP, an ATP-powered unfolding and protein-degradation machine', *Biochimica et Biophysica Acta - Molecular Cell Research*. Elsevier B.V., 1823(1), pp. 15–28. doi: 10.1016/j.bbamcr.2011.06.007.
- Balogh, D. *et al.* (2017) 'Insights into ClpXP proteolysis: heterooligomerization and partial deactivation enhance chaperone affinity and substrate turnover in *Listeria monocytogenes*', *Chemical Science*, 8(2), pp. 1592–1600. doi: 10.1039/c6sc03438a.

- Bewley, M. C. *et al.* (2006) 'The asymmetry in the mature amino-terminus of ClpP facilitates a local symmetry match in ClpAP and ClpXP complexes', *Journal of Structural Biology*, 153(2), pp. 113–128. doi: 10.1016/j.jsb.2005.09.011.
- Bewley, M. C. *et al.* (2009) 'Turned on for degradation: ATPase-independent degradation by ClpP', *Journal of Structural Biology*. Elsevier Inc., 165(2), pp. 118–125. doi: 10.1016/j.jsb.2008.10.005.
- Chien, P. *et al.* (2007) 'Direct and adaptor-mediated substrate recognition by an essential AAA+ protease', *Proceedings of the National Academy of Sciences of the United States of America*, 104(16), pp. 6590–6595. doi: 10.1073/pnas.0701776104.
- Choi, K. H. and Schweizer, H. P. (2006) 'mini-Tn7 insertion in bacteria with single attTn7 sites: Example *Pseudomonas aeruginosa*', *Nature Protocols*, 1(1), pp. 153–161. doi: 10.1038/nprot.2006.24.
- Chua, S. L. *et al.* (2015) 'C-di-GMP regulates *Pseudomonas aeruginosa* stress response to tellurite during both planktonic and biofilm modes of growth', *Scientific Reports*. Nature Publishing Group, 5(March), pp. 1–13. doi: 10.1038/srep10052.
- Crooks, G. *et al.* (2004) 'NCBI GenBank FTP Site WebLogo: a sequence logo generator', *Genome Res*, 14, pp. 1188–1190. doi: 10.1101/gr.849004.1.
- Culp, E. and Wright, G. D. (2017) 'Bacterial proteases, untapped antimicrobial drug targets', *Journal of Antibiotics*. Nature Publishing Group, 70(4), pp. 366–377. doi: 10.1038/ja.2016.138.
- Dahmen, M. *et al.* (2015) 'Structure and mechanism of the caseinolytic protease ClpP1/2 heterocomplex from *Listeria monocytogenes*', *Angewandte Chemie - International Edition*, 54(12), pp. 3598–3602. doi: 10.1002/anie.201409325.
- Dougan, D. A. *et al.* (2002) 'ClpS, a substrate modulator of the ClpAP machine', *Molecular Cell*. Cell Press, 9(3), pp. 673–683. doi: 10.1016/S1097-2765(02)00485-9.
- Drenkard, E. and Ausubel, F. M. (2002) '*Pseudomonas* biofilm formation and antibiotic resistance are linked to phenotypic variation', *Nature*, 416(6882), pp. 740–743. doi: 10.1038/416740a.
- Wagner, V. *et al.* (2003) 'Microarray Analysis of *Pseudomonas aeruginosa* Quorum-Sensing Regulons: Effects of Growth Phase and Environment Microarray Analysis of *Pseudomonas aeruginosa* Quorum-Sensing Regulons: Effects of Growth Phase and

- Environment', *J. Bacteriol.*, 185(7), pp. 2080–2095. doi: 10.1128/JB.185.7.2080.
- Emsley, P. *et al.* (2010) 'Features and development of Coot', *Acta Crystallographica Section D: Biological Crystallography*. International Union of Crystallography, 66(4), pp. 486–501. doi: 10.1107/S0907444910007493.
- Fei, X. *et al.* (2020) 'Structures of the ATP-fueled ClpXP proteolytic machine bound to protein substrate', *eLife*, 9, pp. 1–52. doi: 10.7554/eLife.52774.
- Fernández, L. *et al.* (2012) 'Role of intracellular proteases in the antibiotic resistance, motility, and biofilm formation of *Pseudomonas aeruginosa*', *Antimicrobial Agents and Chemotherapy*, 56(2), pp. 1128–1132. doi: 10.1128/AAC.05336-11.
- Flynn, J. M. *et al.* (2001) 'Overlapping recognition determinants within the *ssrA* degradation tag allow modulation of proteolysis', *Proceedings of the National Academy of Sciences of the United States of America*, 98(19), pp. 10584–10589. doi: 10.1073/pnas.191375298.
- Gatsogiannis, C. *et al.* (2019) 'Cryo-EM structure of the ClpXP protein degradation machinery', *Nature Structural and Molecular Biology*. Springer US, 26(10), pp. 946–954. doi: 10.1038/s41594-019-0304-0.
- Gellatly, S. L. and Hancock, R. E. W. (2013) '*Pseudomonas aeruginosa*: New insights into pathogenesis and host defenses', *Pathogens and Disease*, 67(3), pp. 159–173. doi: 10.1111/2049-632X.12033.
- Gersch, M. *et al.* (2016) 'Barrel-shaped ClpP Proteases Display Attenuated Cleavage Specificities', *ACS Chemical Biology*, 11(2), pp. 389–399. doi: 10.1021/acscchembio.5b00757.
- Gilbert, K. B. *et al.* (2009) 'Global position analysis of the *Pseudomonas aeruginosa* quorum-sensing transcription factor LasR', *Molecular Microbiology*, 73(6), pp. 1072–1085. doi: 10.1111/j.1365-2958.2009.06832.x.
- Gribun, A. *et al.* (2005) 'The ClpP double ring tetradecameric protease exhibits plastic ring-ring interactions, and the N termini of its subunits form flexible loops that are essential for ClpXP and ClpAP complex formation', *Journal of Biological Chemistry*, 280(16), pp. 16185–16196. doi: 10.1074/jbc.M414124200.
- Grimaud, R. *et al.* (1998) 'Enzymatic and structural similarities between the *Escherichia coli* ATP-dependent proteases, ClpXP and ClpAP', *Journal of Biological Chemistry*, 273(20), pp. 12476–12481. doi: 10.1074/jbc.273.20.12476.

- Gur, E., Biran, D. and Ron, E. Z. (2011) 'Regulated proteolysis in Gram-negative bacteria-how and when?', *Nature Reviews Microbiology*. Nature Publishing Group, 9(12), pp. 839–848. doi: 10.1038/nrmicro2669.
- Hall, B. M. *et al.* (2017) 'Two isoforms of Clp peptidase in *Pseudomonas aeruginosa* control distinct aspects of cellular physiology', *Journal of Bacteriology*, 199(3), pp. 1–15. doi: 10.1128/JB.00568-16.
- Hedstrom, L. (2002) 'Serine protease mechanism and specificity', *Chemical Reviews*, 102(12), pp. 4501–4523. doi: 10.1021/cr000033x.
- Hentzer, M. *et al.* (2003) 'Attenuation of *Pseudomonas aeruginosa* virulence by quorum sensing inhibitors', *EMBO J.*, 22(15), pp. 3803–3815.
- Heydorn, A. *et al.* (2000) 'Quantification of biofilm structures by the novel computer program COMSTAT', *Microbiology*, 146(10), pp. 2395–2407. doi: 10.1099/00221287-146-10-2395.
- Hmelo, L. R. *et al.* (2016) 'HHS Public Access', 10(11), pp. 1820–1841. doi: 10.1038/nprot.2015.115.Precision-engineering.
- Hong, Z. *et al.* (2019) 'Azetidine-Containing Alkaloids Produced by a Quorum-Sensing Regulated Nonribosomal Peptide Synthetase Pathway in *Pseudomonas aeruginosa*', *Angewandte Chemie - International Edition*, 58(10), pp. 3178–3182. doi: 10.1002/anie.201809981.
- Joshi, S. A. *et al.* (2004) 'Communication between ClpX and ClpP during substrate processing and degradation', *Nature Structural and Molecular Biology*, 11(5), pp. 404–411. doi: 10.1038/nsmb752.
- Kabsch, W. *et al.* (2010) 'XDS', *Acta Crystallographica Section D Biological Crystallography*, 66(2), pp. 125–132. doi: 10.1107/S0907444909047337.
- Kang, S. G. *et al.* (2004) 'Crystallography and mutagenesis point to an essential role for the N-terminus of human mitochondrial ClpP', *Journal of Structural Biology*, 148(3), pp. 338–352. doi: 10.1016/j.jsb.2004.07.004.
- Kim, Y. I. *et al.* (2001) 'Molecular determinants of complex formation between Clp/Hsp 100 ATPases and the ClpP peptidase', *Nature Structural Biology*, 8(3), pp. 230–233. doi: 10.1038/84967.
- Kimber, M. S. *et al.* (2010) 'Structural and Theoretical Studies Indicate that the Cylindrical Protease ClpP Samples Extended and Compact Conformations', *Structure*. Elsevier Ltd,

- 18(7), pp. 798–808. doi: 10.1016/j.str.2010.04.008.
- Lambertsen, L., Sternberg, C. and Molin, S. (2004) ‘Mini-Tn7 transposons for site-specific tagging of bacteria with fluorescent proteins’, *Environmental Microbiology*, 6(7), pp. 726–732. doi: 10.1111/j.1462-2920.2004.00605.x.
- Letunic, I. and Bork, P. (2019) ‘Interactive Tree Of Life (iTOL) v4: recent updates and new developments’, *Nucleic acids research*. Oxford University Press, 47(W1), pp. W256–W259. doi: 10.1093/nar/gkz239.
- Liu, K., Ologbenla, A. and Houry, W. A. (2014) ‘Dynamics of the ClpP serine protease: A model for self-compartmentalized proteases’, *Critical Reviews in Biochemistry and Molecular Biology*, 49(5), pp. 400–412. doi: 10.3109/10409238.2014.925421.
- Lopez, K. E. *et al.* (2020) ‘Conformational plasticity of the ClpAP AAA+ protease couples protein unfolding and proteolysis’, *Nature Structural and Molecular Biology*. Springer US, 27(5), pp. 406–416. doi: 10.1038/s41594-020-0409-5.
- Lyczak, J. B., Cannon, C. L. and Pier, G. B. (2000) ‘Establishment of *Pseudomonas aeruginosa* infection: Lessons from a versatile opportunist’, *Microbes and Infection*, 2(9), pp. 1051–1060. doi: 10.1016/S1286-4579(00)01259-4.
- Maglica, Ž., Kolygo, K. and Weber-Ban, E. (2009) ‘Optimal Efficiency of ClpAP and ClpXP Chaperone-Proteases Is Achieved by Architectural Symmetry’, *Structure*, 17(4), pp. 508–516. doi: 10.1016/j.str.2009.02.014.
- Mah, T. F. *et al.* (2003) ‘A genetic basis for *Pseudomonas aeruginosa* biofilm antibiotic resistance’, *Nature*, 426(6964), pp. 306–310. doi: 10.1038/nature02122.
- Maurizi, M. R. *et al.* (1994) ‘Endopeptidase Clp: ATP-dependent Clp protease from *Escherichia coli*’, *Methods in Enzymology*, 244(C), pp. 314–331. doi: 10.1016/0076-6879(94)44025-5.
- Maurizi, M. R. *et al.* (1998) ‘Molecular Properties of ClpAP Protease of *Escherichia coli*: ATP-Dependent Association of ClpA and ClpP’, *Biochemistry*, 37(21), pp. 7778–7786. doi: 10.1021/bi973093e.
- McCoy, A. J. *et al.* (2007) ‘Phaser crystallographic software’, *Journal of Applied Crystallography*. International Union of Crystallography, 40(4), pp. 658–674. doi: 10.1107/S0021889807021206.
- Nørby, J. G. (1988) ‘Coupled Assay of Na⁺,K⁺-ATPase Activity’, *Methods in Enzymology*, 156(C), pp. 116–119. doi: 10.1016/0076-6879(88)56014-7.

- Olivares, A. O. *et al.* (2014) ‘Mechanochemical basis of protein degradation by a double-ring AAA+ machine’, *Nature Structural and Molecular Biology*. Nature Publishing Group, 21(10), pp. 871–875. doi: 10.1038/nsmb.2885.
- Ortega, J. *et al.* (2002) ‘Alternating translocation of protein substrates from both ends of ClpXP protease’, *EMBO Journal*, 21(18), pp. 4938–4949. doi: 10.1093/emboj/cdf483.
- Otwinowski, Z. and Minor, W. (1997) ‘Processing of X-Ray Diffraction Data Collected in Oscillation Mode’, *Methods in Enzymology*, 276(20), pp. 307–326. doi: [https://doi.org/10.1016/S0076-6879\(97\)76066-X](https://doi.org/10.1016/S0076-6879(97)76066-X).
- Pan, S. *et al.* (2019) ‘The functional ClpXP protease of *Chlamydia trachomatis* requires distinct clpP genes from separate genetic loci’, *Scientific Reports*. Springer US, 9(1), pp. 1–14. doi: 10.1038/s41598-019-50505-5.
- Patteson, J. B., Lescalette, A. R. and Li, B. (2019) ‘Discovery and Biosynthesis of Azabicyclene, a Conserved Nonribosomal Peptide in *Pseudomonas aeruginosa*’, *Organic Letters*, 21(13), pp. 4955–4959. doi: 10.1021/acs.orglett.9b01383.
- Qiu, D. *et al.* (2008) ‘ClpXP proteases positively regulate alginate overexpression and mucoid conversion in *Pseudomonas aeruginosa*’, *Microbiology*, 154(7), pp. 2119–2130. doi: 10.1099/mic.0.2008/017368-0.
- Ripstein, Z. A. *et al.* (2020) ‘A processive rotary mechanism couples substrate unfolding and proteolysis in the ClpXP degradation machinery’, *eLife*, 9:e52158. doi:10.7554/eLife.52158.
- Sauer, R. T. and Baker, T. A. (2011) ‘AAA+ Proteases: ATP-Fueled Machines of Protein Destruction’, *Annual Review of Biochemistry*, 80(1), pp. 587–612. doi: 10.1146/annurev-biochem-060408-172623.
- Schechter, I. and Berger, A. (1972) ‘On the size of the active site in proteases’, *Biochemical and Biophysical Research Communications*, 46(5), pp. 1956–1960. doi: 10.1016/0006-291X(72)90076-9.
- Schuster, M. *et al.* (2003) ‘(4916) Identification, Timing, and Signal Specificity of *Pseudomonas aeruginosa* Quorum-controlled Genes: a Transcriptome Analysis’, *J. Bacteriol.*, 185(7), pp. 2066–2079. doi: 10.1128/JB.185.7.2066.
- Shanks, R. M. Q. *et al.* (2006) ‘*Saccharomyces cerevisiae*-based molecular tool kit for manipulation of genes from Gram-negative bacteria’, *Applied and Environmental*

- 831 *Microbiology*, 72(7), pp. 5027–5036. doi: 10.1128/AEM.00682-06.
- 832 Sievers, F. *et al.* (2011) ‘Fast, scalable generation of high-quality protein multiple sequence
833 alignments using Clustal Omega’, *Molecular Systems Biology*, 7(539). doi:
834 10.1038/msb.2011.75.
- 835 Stanne, T. M. *et al.* (2007) ‘Distinctive types of ATP-dependent Clp proteases in Cyanobacteria’,
836 *Journal of Biological Chemistry*. doi: 10.1074/jbc.M700275200.
- 837 Szyk, A. and Maurizi, M. R. (2006) ‘Crystal structure at 1.9 Å of *E. coli* ClpP with a peptide
838 covalently bound at the active site’, *Journal of Structural Biology*, 156(1), pp. 165–174.
839 doi: 10.1016/j.jsb.2006.03.013.
- 840 Thompson, M. W., Singh, S. K. and Maurizi, M. R. (1994) ‘Processive degradation of proteins by
841 the ATP-dependent Clp protease from *Escherichia coli*. Requirement for the multiple array
842 of active sites in ClpP but not ATP hydrolysis’, *Journal of Biological Chemistry*, 269(27),
843 pp. 18209–18215.
- 844 Waite, R. D. *et al.* (2006) ‘Clustering of *Pseudomonas aeruginosa* transcriptomes from planktonic
845 cultures, developing and mature biofilms reveals distinct expression profiles’, *BMC*
846 *Genomics*, 7, pp. 1–14. doi: 10.1186/1471-2164-7-162.
- 847 Zhao, J. *et al.* (2016) ‘Structural and Molecular Mechanism of CdpR Involved in Quorum-Sensing
848 and Bacterial Virulence in *Pseudomonas aeruginosa*’, *PLoS Biology*, 14(4), pp. 1–25. doi:
849 10.1371/journal.pbio.1002449.

Figure Legends

Figure 1: PaClpP1 and PaClpP2 co-immunoprecipitate from *P. aeruginosa* and *E. coli*.

- A) Schematic of ATP-dependent proteolysis by PaClpXP₁₄. PaClpX₆ is shown in purple, PaClpP1 is shown in blue.
- B) Schematic of ATP-dependent proteolysis by PaClpP1₇P2₇. Color scheme is the same as in A), except PaClpP2 is shown in cyan.
- C) ClpP2-FLAG was isolated from cell lysates of PAO1 containing either *clpP2-FLAG* (lane C), untagged *clpP2* (lane A), or *clpP2^{S98A}-FLAG* alleles using anti-FLAG antibody-conjugated beads and elution with excess FLAG peptide (Sigma-Aldrich). Eluate was separated by SDS-PAGE and proteins were stained with SYPRO orange (lanes E-F). Molecular weight standards are shown in lane A. Molecular weights of monomers: ClpP2-FLAG, 23,237 Da; ClpP1, 21,879 Da.
- D) The eluate was analyzed by Western blot for PaClpP1 (1:15,000 anti-PaClp1) and PaClpP2 (1:7,500 anti-PaClpP2). Secondary antibody: goat anti-rabbit (1:10,000).
- E) Gel filtration profile of PaClpP1₇P2₇. Peak fractions corresponding to tetradecamers (58-64 mL, as indicated by dotted lines) were pooled and concentrated for biochemical analysis.
- F) ClpP1 and ClpP2 co-associate during purification. SDS-PAGE of elution fractions. Lanes 1-10 correspond to samples taken from 1 mL fractions eluting from 56-66 mL. Elution fractions corresponding to lanes 3-9 were pooled and concentrated for further characterization. Molecular weights of monomers: ClpP1-His₆, 23,063 Da; ClpP2-StrepII, 23,326 Da.

Figure 2: Crystal structures of PaClpP1₁₄ and PaClpP2₇ complexes.

- A) Side and top-down views of homomeric PaClpP1 (PDB code: 5BQV, blue, with a single monomer in purple).
- B) Side and top-down views of homomeric PaClpP2 (PDB code: 5BQW, deep teal, with a single monomer in yellow).
- C) Overlay of PaClpP1 (blue) and PaClpP2 (cyan) monomers with insets showing select structural differences.
- D) N-termini of PaClpP1 and PaClpP2. The first 13 residues of PaClpP2 and the first four residues of PaClpP1 are missing electron density.
- E) The C-terminus of PaClpP2 adopts a single helical turn, while the C-terminus of PaClpP1 is unstructured. The side chains of the amino acids making up the docking site for AAA+ unfoldases (hydrophobic binding pocket) are represented as black sticks.

F) Active sites. The active site residues of PaClpP1 are properly aligned (distances in angstroms are labeled on figure), while the residues of ClpP2 are not (the distances from PaClpP2 S98 to H123 and H123 to D172 are 6.5Å and 10.1Å, respectively). Residue numbers in blue refer to the mature amino acid sequence of PaClpP1, and residue numbers in cyan refer to the amino acid sequence of PaClpP2.

Figure 3: Both PaClpP1₇ and PaClpP1₇P2₇ form active proteases.

- A) Degradation of GFP-ssrA by PaClpX₆ (0.1 μM) and PaClpP1₁₄ (filled circles) or PaClpP1₇P2₇ (open triangles) (0.54 μM). Curves are fit to the Michaelis-Menten equation. Solid line refers to PaClpX•ClpP1₁₄ ($K_M = 4.2 \pm 0.5 \mu\text{M}$, $V_{\max} = 1.6 \pm 0.08 \text{ min}^{-1} \text{ ClpX}_6^{-1}$) and dotted line refers to PaClpX•ClpP1₇P2₇ ($K_M = 4.1 \pm 0.52 \mu\text{M}$, $V_{\max} = 1.7 \pm 0.09 \text{ min}^{-1} \text{ ClpX}_6^{-1}$).
- B) Degradation of 50 μM FITC-casein (Casein fluorescein isothiocyanate) by 0.4 μM PaClpP1₁₄ or PaClpP1₇P2₇ and 0.2 μM PaClpA₆. For both (A) and (B), data points are averages of three independent replicates performed in duplicate ± SD.
- C) Negative-stain microscopy images of PaClpX₆ (0.5 μM) with PaClpP1₁₄ or PaClpP1₇P2₇ (0.2 μM). Approximately half of the PaClpX•P1₁₄ complexes were doubly-capped by PaClpX (left; 46% doubly-capped, 54% singly-capped), whereas most PaClpX•ClpP1₇P2₇ complexes were singly-capped (right; 98% singly-capped). Representative doubly- and singly-capped complexes are circled with dotted and solid lines, respectively.
- D) Efficient degradation of GFP-ssrA (8 μM) requires productive interaction of PaClpX₆ (0.5 μM) with the PaClpP1₇ ring of PaClpP1₇P2₇. Wild-type PaClpP1₁₄ or PaClpP1₇P2₇ (2 μM) with PaClpX degrades GFP-ssrA, whereas the PaClpX-binding-defective variant of PaClpP1₁₄ (R194K) was not able to support degradation of GFP-ssrA in a heterocomplex with PaClpP2₇ (PaClp^{RK}P1₇P2₇). Data points are averages of three independent replicates performed in triplicate ± SD.
- E) Violin plots of GFP-ssrA degradation by PaClpX•ClpP1₁₄ and PaClpX•ClpP1₇P2₇. The rate of GFP-ssrA (8 μM) degradation is dependent upon the amount of PaClpP₇-bound PaClpX₆. 2:1 complex formation was favored under conditions containing 1.0 μM PaClpX₆ and 0.5 μM of PaClpP1₁₄, while 1:1 stoichiometries were favored under conditions containing 1.0 μM PaClpX₆ and 1.0 μM PaClpP1₁₄, 0.5 μM PaClpP1₇P2₇, or 1.0 μM PaClpP1₇P2₇.

Figure 4: The active site of PaClpP2 is essential for robust biofilm development in *P. aeruginosa* PAO1.

- A) Representative side-view confocal images of GFP-labeled PAO1 biofilms grown in 96-well glass-bottom plates under static conditions for 48 hours. Strains are either wild type, $\Delta clpP1$, $\Delta clpP2$, or contain a FLAG-tagged catalytic-null allele of *clpP2* in lieu of the wild-type gene (*clpP2*^{S98A}-flag).

B-C) Quantifications are averages of three independent wells, with five z-stacks taken per well. Error bars are \pm SEM. Biofilm quantification was performed using COMSTAT software (Heydorn et al., 2000). * $p < 0.0001$ as analyzed by one-way ANOVA.

Figure 5: The PaClpP1₇ and PaClpP2₇ active sites of PaClpP1₇P2₇ contribute uniquely to peptide cleavage.

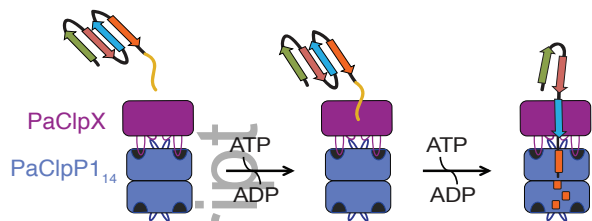
- A) Schematic of assays used for the determination of cleavage-site specificity by PaClpP₁₄ complexes.
- B) Cleavage of a panel of 18 fluorescent peptide substrates (100 μ M) by PaClpP₁₄ or PaClpP₁₇P2₇ (0.4 μ M) at 30°C. Substrates are ordered by the properties of the amino acid at position P1' (from left to right: small to large, and non-polar to charged). Data points are averages of three independent replicates performed in duplicate \pm SD.
- C) The PaClpP2₇ active sites contribute to peptide hydrolysis. PaClp^{SAP}P₁₇P2₇ is a partially-inactive variant of PaClpP₁₇P2₇ in which the active serine of PaClpP1 is mutated to alanine. Peptide substrates are ordered as in (B). Peptidase activity is normalized to PaClpP₁₄.
- D) Percent contribution of PaClpP2₇ activity to total peptidase activity in PaClpP₁₇P2₇. Relative peptidase activities of PaClp^{SAP}P₁₇P2₇ for each substrate were divided by the relative peptidase activities of the wild-type heterocomplex for that substrate. Substrates are ranked from left to right based on decreasing sensitivity to PaClpP2₇ cleavage.
- E-H) More than 13,000 proteolytic products spanning four substrates (GFP-ssrA, FNR-ssrA, arc-GCN4p1-st11-ssrA, and Halo-(V15P titin^{I27})₄-ssrA) were sequenced by mass spectrometry and compiled to create WebLogos. (E) Motif generated from PaClpX•ClpP₁₄ complexes. (F) Motif generated by PaClpX•ClpP₁₇^{SAP}P2₇ complexes. (G) Motif generated by PaClpX•Clp^{SAP}P₁₇P2₇ complexes. (H) Motif generated by PaClpX•ClpP₁₇P2₇ complexes.

Figure 6: Summary and models for PaClpP1 and PaClpP2 assemblies and functions.

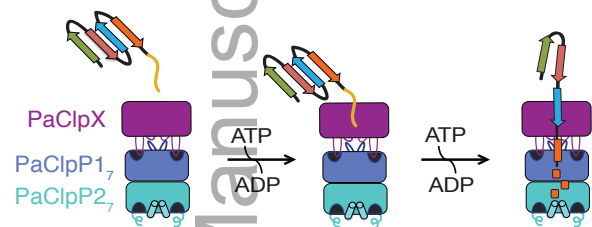
- A) Graphical summary of the oligomeric states and biochemical activities of PaClpP₁₄, PaClpP2₇, and PaClpP₁₇P2₇. Whereas PaClpP2₇ is an inactive heptamer, PaClpP₁₄ and PaClpP₁₇P2₇ are active tetradecamers that can interact with PaClpX and PaClpA to degrade model substrates. PaClpP₁₇P2₇ binds asymmetrically to PaClpX (right panel), whereas PaClpP₁₄ can bind two equivalents of PaClpX₆ (i.e., can be doubly-capped). PaClpP₁₇P2₇ promotes biofilm thickness, whereas PaClpP1 impacts motility, biofilm formation, and phenazine production *in vivo* (¹Hall et al, 2017; ²Zhao et al., 2016; ³This study, and Shanks et al., 2006).
- B) Models for *in vivo* functions of PaClpP₁₇P2₇. The left panel shows an ATPase-independent model for PaClpP₁₇P2₇ activity, in which a small propeptide can diffuse into the axial pore of the heterocomplex

and be cleaved by PaClpP₁₇P₂₇ to produce an active peptide product. The right panel depicts an ATPase-dependent function of PaClpP₁₇P₂₇, where a biologically important proteolytic product is generated by unfoldase-coupled PaClpP₁₇P₂₇. Both (A) and (B) represent models in which a currently unknown target with a functional role in biofilm architecture is produced via cleavage by PaClpP₁₇P₂₇.

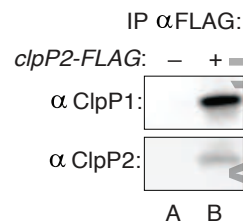
A.



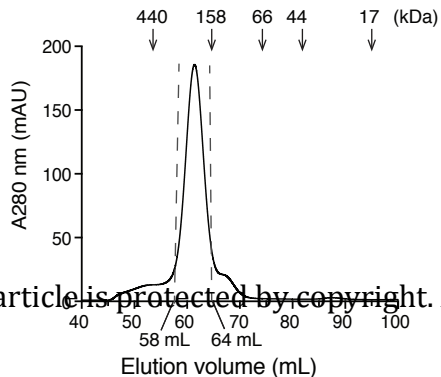
B.



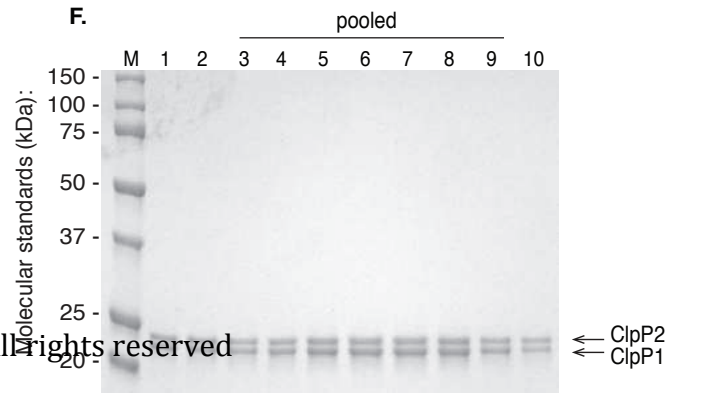
D.



E.



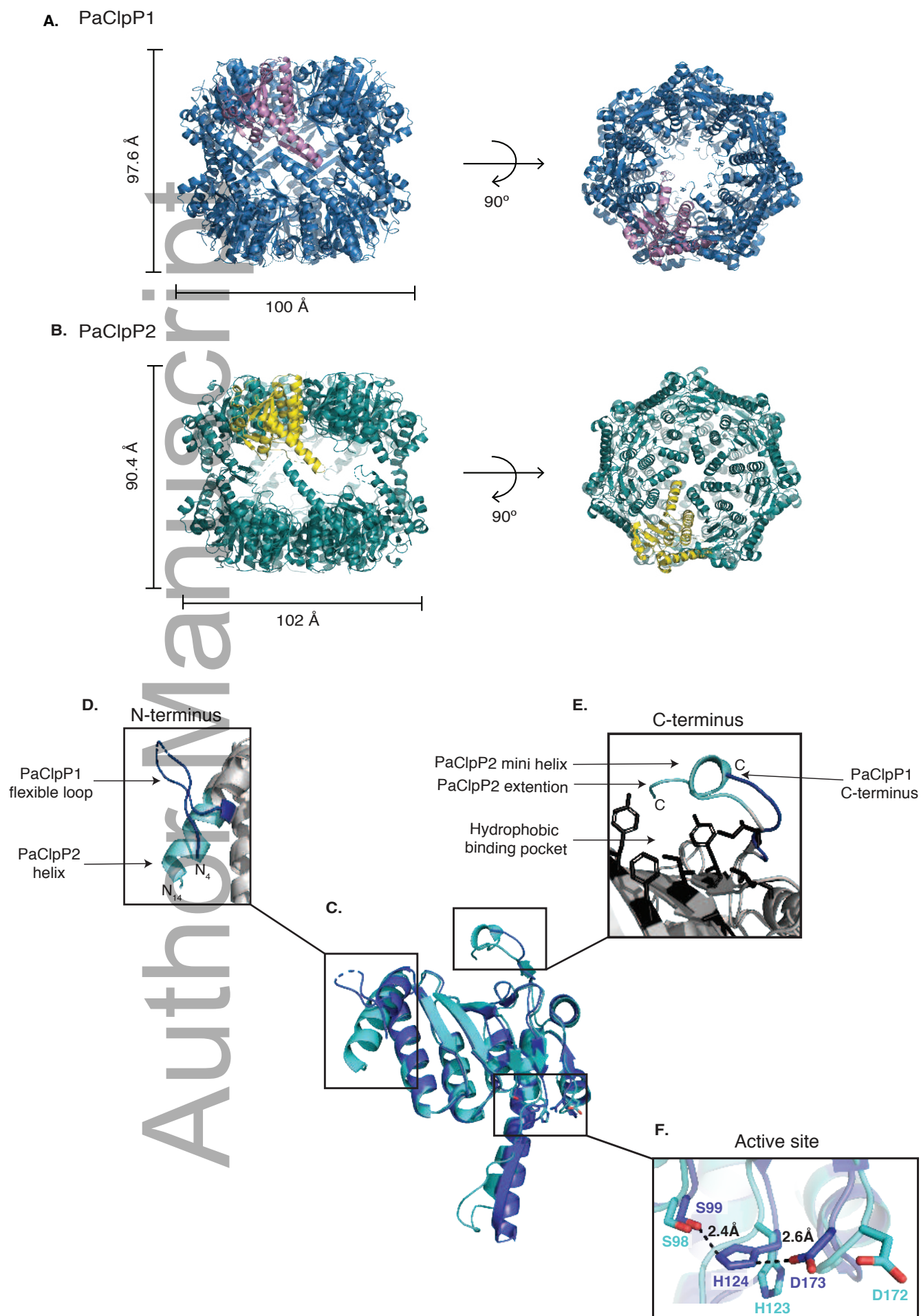
F.



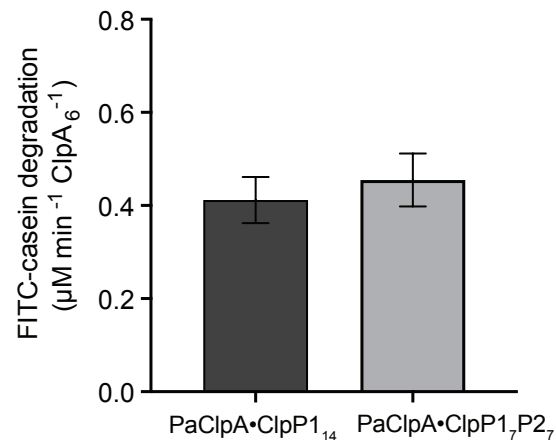
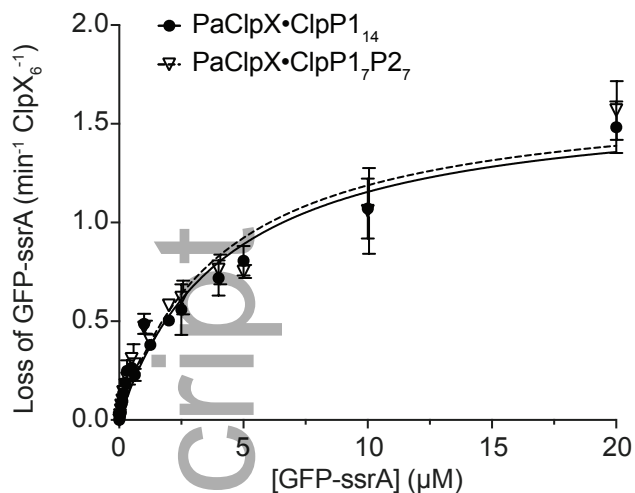
Molecular standards (kDa):

Lanes: A B C D E F G

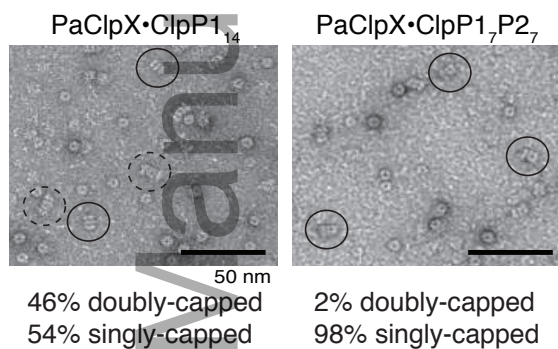
← ClpP2-FLAG
← ClpP1



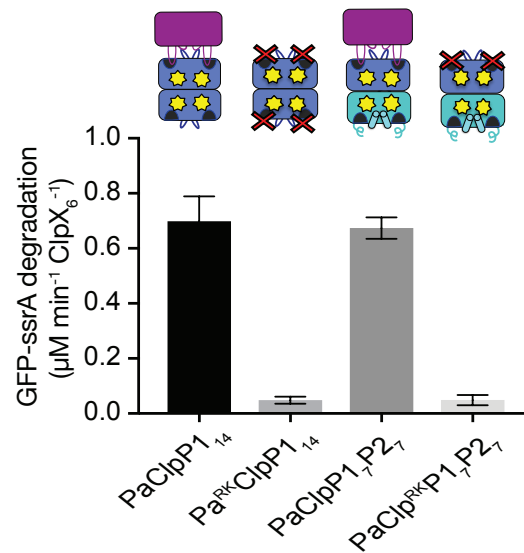
A.



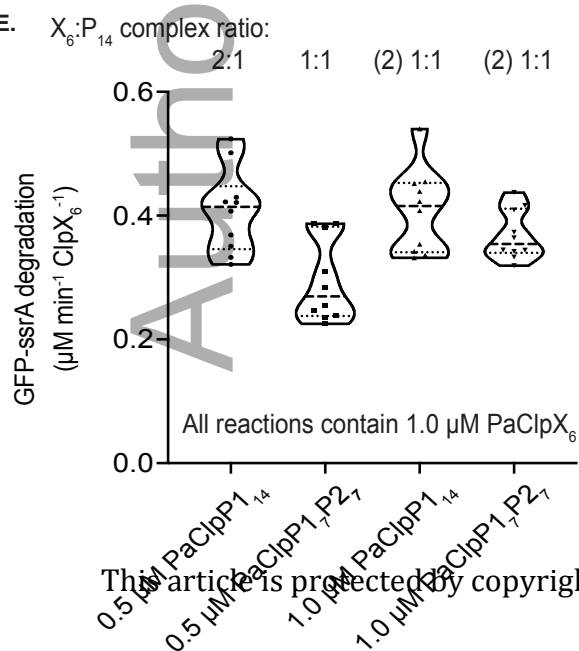
C.



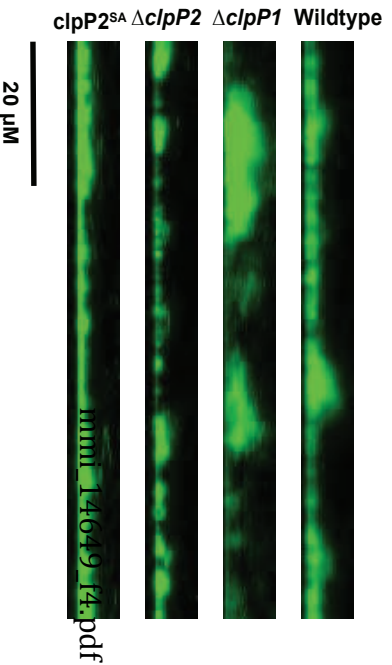
D.



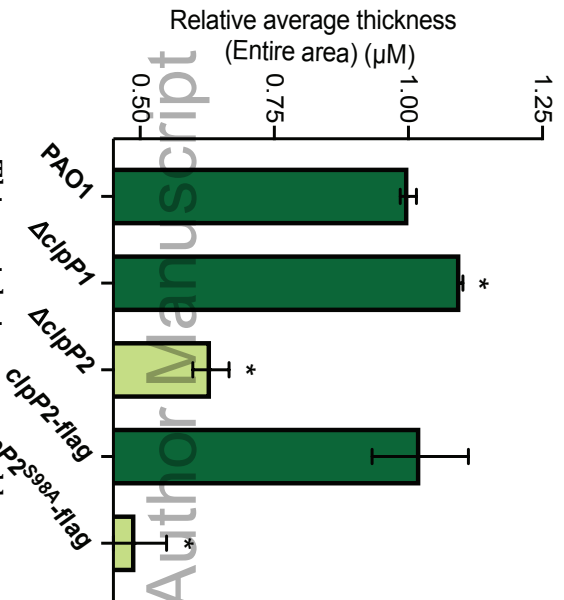
E.

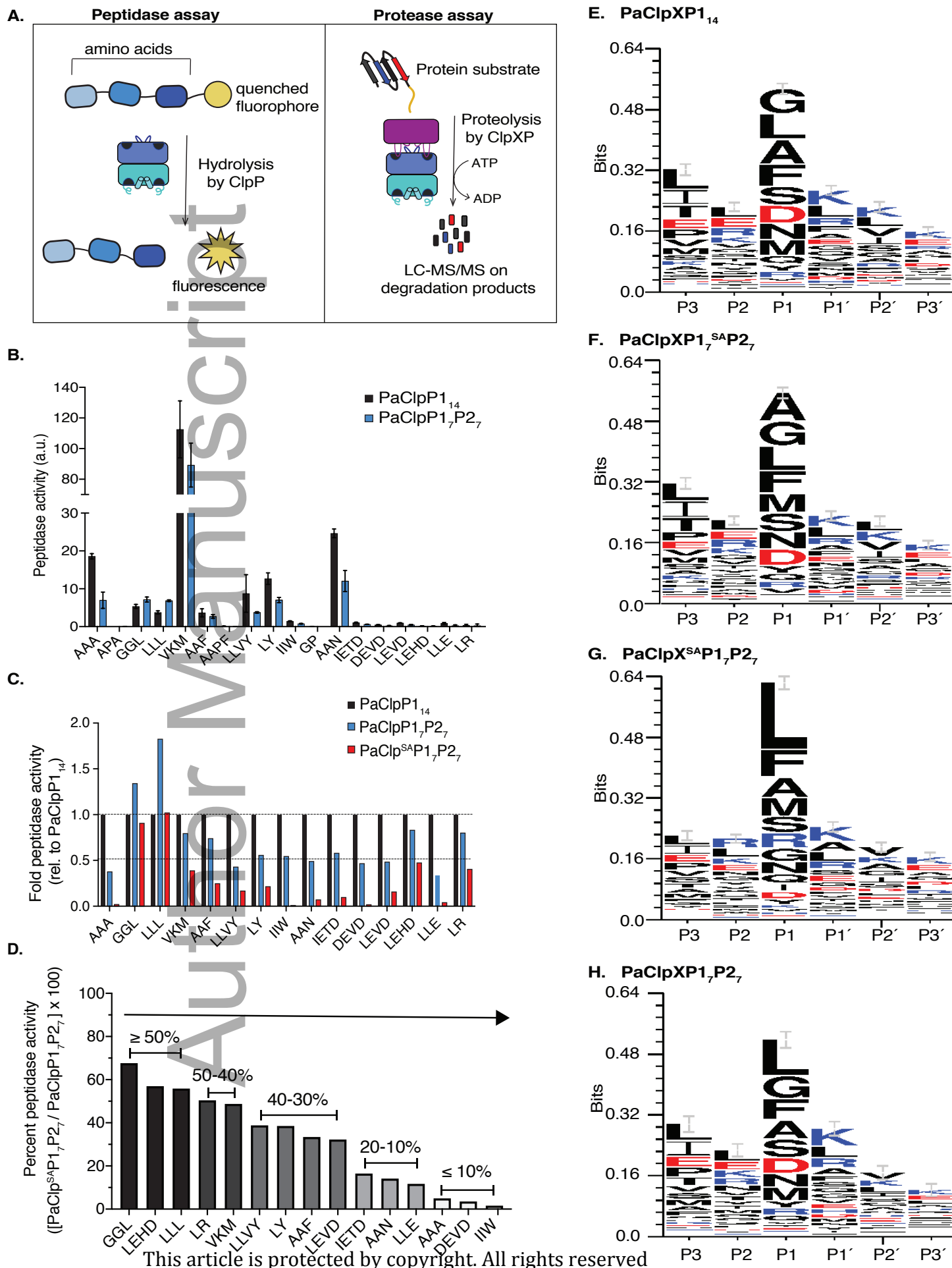


A.

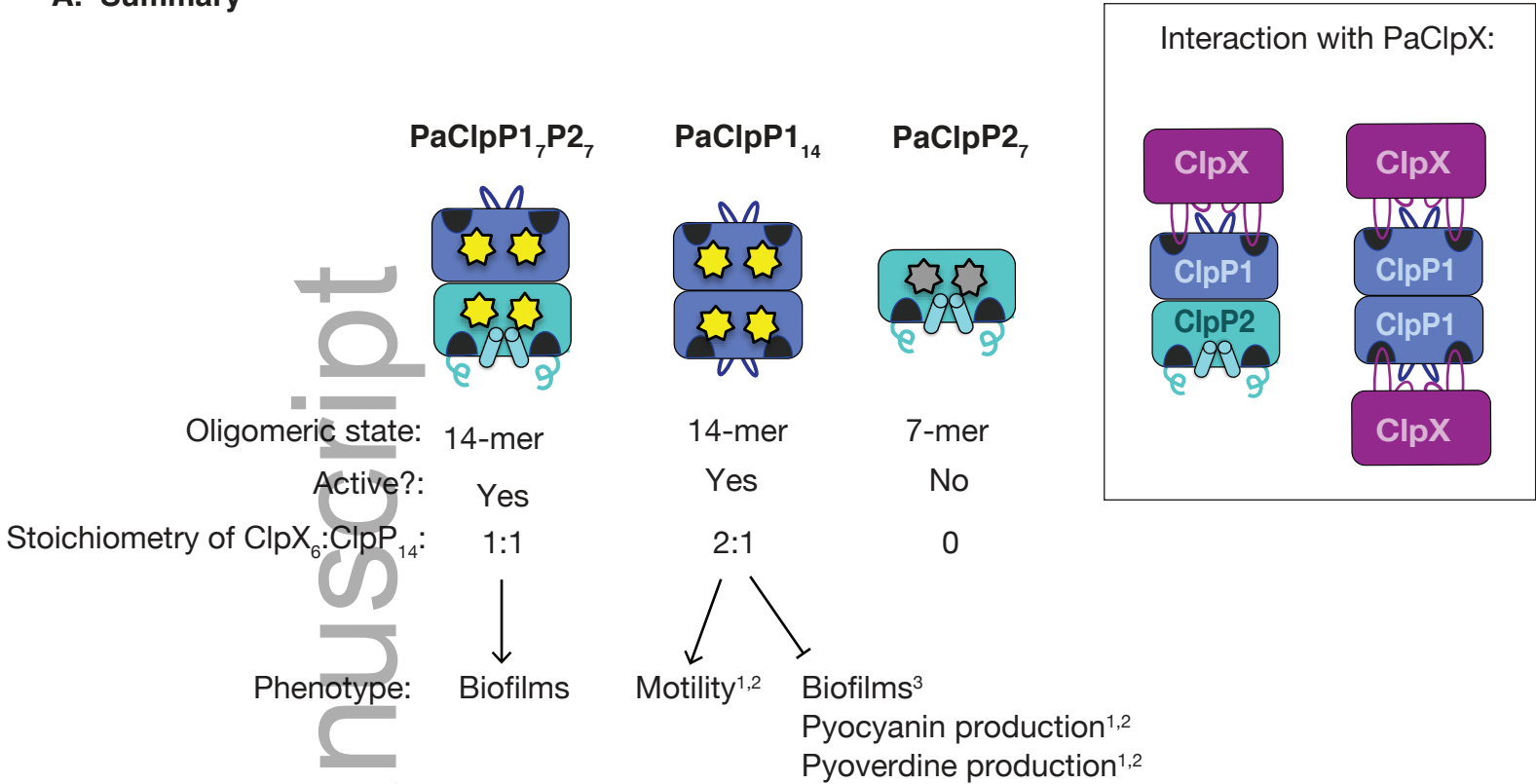


B.





A. Summary



B. Models

Peptide processing event by PaClpP1₇P2₇
(ATPase-independent)

Proteolytic product generation by PaClpP1₇P2₇
(ATPase-dependent)

